69th International Astronautical Congress, Bremen, Germany. Copyright © 2018 by the authors. All rights reserved.

IAC–18–C1.1.8

Low-Thrust Trajectory Design Via Direct Transcription Leveraging Structures from the Low-Thrust Restricted Problem

Robert Pritchett
Purdue University, USA, pritcher@purdue.edu

Andrew D. Cox
Purdue University, USA, cox50@purdue.edu

Kathleen C. Howell
Purdue University, USA, howell@purdue.edu

David C. Folta
NASA Goddard Space Flight Center, USA, david.c.folta@nasa.gov

Daniel Grebow
Jet Propulsion Laboratory - California Institute of Technology, USA, daniel.grebow@jpl.nasa.gov

A primary challenge of low-thrust mission design is the development of an initial guess for the state and control history of a trajectory. To address this challenge, one technique assembles dynamical structures, such as periodic orbits and their associated manifolds, into discontinuous chains that are corrected to locally optimal transfer solutions via direct transcription. In this investigation, dynamical structures that leverage low-thrust in a multi-body regime are incorporated into the orbit chain approach to expand the options available for construction of an initial guess and to guide the direct transcription algorithm toward different categories of locally optimal solutions. The properties and structures of the low-thrust model which facilitate orbit chain construction are demonstrated in representative transfer scenarios. Direct transcription is applied to converge upon locally optimal transfer trajectories in both simplified and ephemeris models. Results indicate that low-thrust dynamical structures offer a promising new catalog of options for use in the orbit chain approach to designing optimal low-thrust trajectories.

I. Introduction

The efficiency of low-thrust propulsion has enabled a variety of ambitious missions in recent decades[1,2] and spurred the proposal of many new ones that will leverage this technology to explore the solar system.[3–5] The growing use of low-thrust propulsion necessitates that methods to design and navigate low-thrust trajectories be improved. One of the primary challenges of low-thrust mission design is the development of an appropriate initial guess for the combined state and control history of a trajectory. While many strategies exist to leverage dynamical structures in two- and three-body models for ballistic trajectory design, fewer methods are available to supply an initial control history. This investigation seeks to leverage structures from a combined low-thrust, multi-body model to facilitate such preliminary planning. By including these structures in a direct transcription scheme, low-thrust transfers between various regions of the three-body system are designed and validated.

One technique for addressing the challenge of low-thrust trajectory design assembles dynamical structures, such as periodic orbits and their associated manifolds, into discontinuous chains that are corrected to locally optimal transfer solutions via direct transcription.[6,7] Typically, the links employed in this orbit chain approach are ballistic trajectories, and thrust arcs are added during the corrections process to facilitate convergence and remove discontinuities between links. However, employing only natural arcs in an initial guess may obscure families of mass or time optimal trajectories that possess different geometries and control histories. One strategy that may mitigate this possibility is the incorporation of dynamical structures that leverage low-thrust into the orbit chain approach. These additional structures expand the options available for the construction of an initial guess and guide the direct transcription algorithm toward alternative sets of locally optimal solutions. In this work, a low-thrust (LT) force is added to the equations that define the circular re-

stricted three-body problem (CR3BP) to construct a combined model, the CR3BP-LT. Techniques from dynamical systems theory are applied to gain insight into the combined dynamics and to generate a variety of useful structures. Representative transfer scenarios demonstrate how these structures facilitate orbit chain construction by supplying new geometries and reducing state discontinuities between links. Furthermore, insights from the CR3BP-LT model inform the selection of arcs included in an orbit chain and guide the formulation of the initial control history. Following orbit chain assembly, direct transcription is applied to converge upon locally optimal transfer trajectories in the CR3BP. Finally, the optimal paths are transitioned to a high-fidelity model for validation. Results indicate that an orbit chain containing low-thrust dynamical structures is equally as capable of delivering an optimal low-thrust trajectory as one that contains only ballistic structures. Moreover, a method employing low-thrust dynamical structures is adaptable, because these structures can be generated for a wide variety of system and spacecraft models as well as many different transfer scenarios. The application of low-thrust structures is particularly useful for transfer design between stable or nearly stable orbits that do not possess natural manifolds to facilitate flow to and from the orbits. Overall, low-thrust dynamical structures offer a promising new catalog of options for use in the orbit chain approach to designing optimal low-thrust trajectories.

II. Background

Multiple authors have explored techniques for low-thrust trajectory design similar to the chaining approach leveraged in this investigation.[6,7] For example, Howell, Barden, and Lo apply this strategy in the context of the CR3BP to link invariant manifolds between periodic orbits for what became the GENESIS mission.[8] This application of dynamical systems theory to trajectory design has been further developed by a variety of researchers who utilize invariant manifolds to form *dynamical chains* that reveal natural flow in a wide range of three-body systems, and facilitate transfer design.[9–13] Parker and others similarly employ a chaining approach to link periodic orbits and their manifolds to form complex new periodic orbits.[14,15] Recently, Restrepo and Russell have presented a method of "Patched Periodic Orbits" that leverages an extensive database of periodic orbits[16] to quickly design low-energy transfers throughout the CR3BP by patching together successive periodic orbits.[17] While the work of these authors includes many different applications, each employs a chaining strategy to link dynamical structures, as this is a straightforward and practical approach to trajectory design. The present investigation builds upon these developments and seeks to further alleviate the challenge of low-thrust trajectory design in the CR3BP by assembling chains of ballistic and low-thrust dynamical structures.

Although many strategies exist to assemble and adjust chains of dynamical structures, collocation offers several distinct advantages. Collocation is an implicit numerical integration method that approximates the solution to a set of ordinary differential equations using polynomials. This approach is particularly robust compared to other methods, because collocation algorithms are often able to converge upon a solution given a poor initial guess even when other techniques fail. When paired with an optimization algorithm, the resulting scheme is denoted *direct transcription.*[18] In this scheme, collocation is employed to discretize a continuous optimal control problem into a nonlinear programming problem (NLP) that is then solved via a direct optimization approach. Grebow and Pavlak[19] offer an overview of the history of collocation and direct transcription methods, and these techniques are discussed more generally within several excellent survey papers on the topic of trajectory optimization.[20–22] Many possible implementations of a direct transcription scheme are available; this investigation generally follows the collocation and mesh refinement framework defined by Grebow and Pavlak[19], and is consistent with previous work.[6,7] Direct transcription has been leveraged previously to explore solutions to low-thrust trajectory design problems in the Earth-Moon CR3BP.[23–26] This earlier work demonstrates that direct transcription successfully delivers a solution for a wide range of initial guess and path constraint scenarios. Overall, the robustness and adaptability of direct transcription offers a powerful strategy for computing low-thrust solutions.

Although direct transcription possesses a wide basin of convergence, the generation of initial guesses for low-thrust paths through multi-body regimes remains challenging and can negatively influence the results obtained from collocation. While there are many strategies for designing thrust vector histories in the two-body problem[27,28], fewer methods incorporate multi-body dynamics. Studies of solar sail dynamics in the Earth-Sun and Earth-Moon three-body systems supply some guidance on the selection of sail parameters to achieve stable orbits around arti-

ficial equilibria[29], or paths between sequences of artificial equilibria.[30] Subsequent studies of the combined CR3BP-solar sail dynamics reveal a rich variety of dynamical structures, including invariant manifolds, periodic orbits, and quasi-periodic orbits.[31,32] Similar structures exist in a more general low-thrust, multi-body model, the CR3BP-LT, and are leveraged to identify initial guesses for the low-thrust control history.[33,34] Dynamical structures and insights from the low-thrust CR3BP (CR3BP-LT) are employed in this investigation to construct initial designs that incorporate low-thrust.

III. Dynamical Model Development

The first step in computing and leveraging dynamical structures for inclusion in a low-thrust trajectory design is the development of the dynamical model. An energy-based approach is first employed to derive the governing equations in the CR3BP and obtain an expression for the natural Hamiltonian. By augmenting the CR3BP equations of motion (EOMs) with a low-thrust term, the CR3BP-LT is constructed and the associated low-thrust Hamiltonian is defined. This low-thrust Hamiltonian serves as an integral of motion when the low-thrust acceleration vector is fixed in the rotating frame, and, thus, may be leveraged to characterize motion in the CR3BP-LT. Finally, transfers constructed within the CR3BP are transitioned to an N-body ephemeris model for validation.

III.i Circular Restricted Three-Body Problem

The CR3BP describes the motion of a relatively small body, such as a spacecraft, in the presence of two larger gravitational point masses (P_1 and P_2) with paths that evolve along circular orbits about their mutual barycenter (B). To simplify the governing equations and enable straightforward visualization of periodic solutions, the motion of the spacecraft is described in a right-handed frame ($\hat{x},\ \hat{y},\ \hat{z}$) that rotates with the two primaries, as seen in Figure 1, where $\hat{x}$, $\hat{y}$, and $\hat{z}$ are vectors of unit length (denoted by the caret above the symbol). The system is parameterized by the mass ratio, $\mu = M_2/(M_1+M_2)$, where M_1 and M_2 are the masses of the primaries and $M_1 \geq M_2$. To facilitate numerical integration, the dimensional values are nondimensionalized by characteristic quantities such that the distance between P_1 and P_2 is unity, the mean motion of the two primaries is unity, and the masses of each body range from zero to one.[35]

The equations of motion governing the CR3BP are

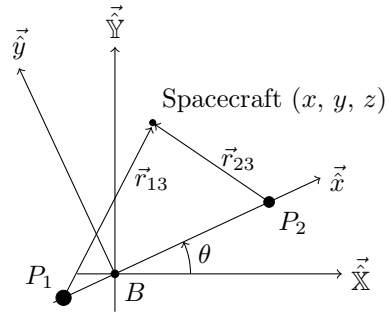

Fig. 1: CR3BP system configuration; two point masses, P_1 and P_2, proceed on circular orbits about their mutual barycenter, B. The behavior of a third, relatively massless particle is described via the rotating coordinate frame, ($\hat{x},\ \hat{y},\ \hat{z}$)

derived via a Hamiltonian energy approach. Let the kinetic (T) and potential (V) energies corresponding to the CR3BP system be defined by

$$T = \frac{1}{2}\left[(\dot{x}-y)^2 + (\dot{y}+x)^2 + \dot{z}^2\right], \qquad [1]$$

$$V = \frac{-(1-\mu)}{r_{13}} - \frac{\mu}{r_{23}}, \qquad [2]$$

where $\dot{x}$, $\dot{y}$, and $\dot{z}$ are the derivatives of the position states with respect to nondimensional time as observed in the rotating frame, and r_{13} and r_{23} are the distances between the spacecraft (P_3) and the first and second primaries, respectively:

$$r_{13} = \sqrt{(x+\mu)^2 + y^2 + z^2},$$
$$r_{23} = \sqrt{(x-1+\mu)^2 + y^2 + z^2}.$$

Next, form the Hamiltonian,

$$H_{nat} = \frac{1}{2}v^2 - \frac{1}{2}\left(x^2+y^2\right) - \frac{1-\mu}{r_{13}} - \frac{\mu}{r_{23}}, \qquad [3]$$

where $v^2 = \dot{x}^2+\dot{y}^2+\dot{z}^2$ is the spacecraft velocity magnitude in the rotating frame. By applying Hamilton's canonical equations of motion, a set of differential equations that govern the motion of P_3 emerges,

$$\ddot{x} = 2\dot{y} + \Omega_x, \qquad [4]$$
$$\ddot{y} = -2\dot{x} + \Omega_y, \qquad [5]$$
$$\ddot{z} = \Omega_z, \qquad [6]$$

where Ω is the CR3BP *pseudo-potential* function,

$$\Omega = \frac{1}{2}(x^2+y^2) + \frac{1-\mu}{r_{13}} + \frac{\mu}{r_{23}}, \qquad [7]$$

and Ω_x, Ω_y, and Ω_z represent the partial derivatives of Ω with respect to the subscripted variables x, y, and z. Because the CR3BP is autonomous and conservative, H_{nat} is constant and proportional to the Jacobi integral, i.e., the *Jacobi constant*. The Jacobi constant, $C = -2H_{nat}$, is commonly used as a measure of the energy associated with arcs in the CR3BP.

III.ii CR3BP Incorporating Low-Thrust

To incorporate low-thrust into the CR3BP multibody model, the low-thrust acceleration vector is first defined. This vector,

$$\vec{a}_{lt} = \frac{f}{m}\hat{u}\,, \qquad [8]$$

is oriented relative to the rotating frame via the unit vector $\hat{u}$ and scaled by the nondimensional thrust magnitude, f, and nondimensional spacecraft mass, $m = M_3/M_{3,0}$, where M_3 is the instantaneous spacecraft mass and $M_{3,0}$ is the initial (wet) spacecraft mass. A nondimensional thrust magnitude of $f \approx 10^{-2}$ in the Earth-Moon and Sun-Earth CR3BP-LT systems is consistent with current spacecraft capabilities, such as Deep Space 1, Dawn, or Hayabusa.[33,34] Accordingly, a low-thrust acceleration magnitude of $a_{lt} = f/m = 7\text{e-}2$ is frequently employed in this document to represent a reasonable low-thrust capability of about 0.19mm/s^2 in the Earth-Moon system.

To apply an energy-based derivation of the CR3BP-LT EOMs similar to the derivation leveraged for the CR3BP, the CR3BP dynamics are augmented with a low-thrust acceleration term. While the spacecraft kinetic energy expression in Equation [1] remains unchanged, the potential energy expression incorporates a low-thrust acceleration term, i.e.,

$$V_{lt} = \frac{-(1-\mu)}{r_{13}} - \frac{\mu}{r_{23}} - \vec{r}\bullet\vec{a}_{lt}\,, \qquad [9]$$

where $\vec{r} = \{x \quad y \quad z\}^T$. This additional term propagates through the derivation to yield the low-thrust Hamiltonian,

$$H_{lt} = \frac{1}{2}v^2 - \frac{1}{2}\left(x^2+y^2\right) - \frac{1-\mu}{r_{13}} - \frac{\mu}{r_{23}} - \vec{r}\bullet\vec{a}_{lt}\,, \qquad [10]$$

which may also be written in terms of the natural Hamiltonian, i.e.,

$$H_{lt} = H_{nat} - \vec{r}\bullet\vec{a}_{lt}\,. \qquad [11]$$

Due to the time-varying nature of the spacecraft mass, the governing equations are not available directly from Hamilton's canonical equations. However, Newton's law is applied to yield the EOMs,

$$\ddot{x} = 2\dot{y} + \Omega_x + a_{lt}u_x, \qquad [12]$$

$$\ddot{y} = -2\dot{x} + \Omega_y + a_{lt}u_y, \qquad [13]$$

$$\ddot{z} = \Omega_z + a_{lt}u_z, \qquad [14]$$

$$\dot{m} = \frac{-fl_*}{I_{sp}g_0t_*}, \qquad [15]$$

where a_{lt} is the low-thrust acceleration vector magnitude, u_x is the $\hat{x}$-component of $\hat{u}$, etc., I_{sp} is the specific impulse associated with the propulsion system, and $g_0 = 9.80665 \times 10^{-3}$ km/s^2. These equations are consistent with those that govern the natural CR3BP and are augmented with the low-thrust acceleration terms.

To facilitate analyses in the CR3BP-LT, simplifications are applied to reduce the number of dimensions. The natural problem, which is conservative, admits an integral of the motion (the Hamiltonian, H_{nat}), reducing the natural problem dimension by one. Due to the non-autonomous nature of the CR3BP-LT, the low-thrust Hamiltonian is not constant in general and, thus, does not offer a similar dimension reduction. However, when the magnitude and orientation of the low-thrust acceleration vector are fixed in the rotating frame, H_{lt} is constant, yielding a conservative, Hamiltonian system. A constant $\vec{a}_{lt}$ vector is a reasonable assumption in CR3BP-LT systems with sufficiently small l_*/t_* ratios and sufficiently large μ values, such as the Earth-Moon system employed in this investigation.[34] Accordingly, the variable acceleration quantity f/m is replaced by the constant value a_{lt}, removing the need for the mass time-derivative in Equation [15]. These simplifications – a constant low-thrust Hamiltonian and a constant acceleration magnitude – effectively reduce the problem dimension by two.

By leveraging the constant low-thrust acceleration vector simplification, additional insights are available to guide low-thrust trajectory design. While the natural Hamiltonian is not generally constant in the CR3BP-LT, H_{nat} evolves independently of the spacecraft path when $\vec{a}_{lt}$ is fixed in the rotating frame.[34] Finally, to further reduce the system complexity, only planar motion is considered.That is, $z(\tau) = \dot{z}(\tau) = 0$ for all τ, and the planar low-thrust pointing vector, $\hat{u}$, is described by the vector

$$\hat{u} = \left\{\cos\alpha \qquad \sin\alpha \qquad 0\right\}^T\,. \qquad [16]$$

These simplifications facilitate the study of dynamical structures in the CR3BP-LT while also supplying

insights that are useful for spatial (3D) trajectory design.

III.iii N-Body Ephemeris Model

Transfers constructed in a simplified three-body dynamical model must be validated in an N-body ephemeris based model before they can be applied to realistic spaceflight scenarios. The establishment of an ephemeris model begins with the definition of an inertial reference frame. By convention, the origin of this frame is located at the center of one of the gravitational bodies included in the model with mass denoted m_q. The motion of the particle of interest, with mass m_i, is influenced by the central body and expressed within this inertial reference frame. Other gravitational bodies, m_j, included in the ephemeris model exert additional perturbing influences on the particle of interest. All bodies are assumed to be centrobaric point masses, thus, the equations of motion for the particle of interest are,

$$\ddot{\vec{p}}_{qi} = -G\frac{m_i + m_q}{p_{qi}^3}\vec{p}_{qi} + G\sum_{\substack{j=1\\ j\neq i,q}} m_j\left(\frac{\vec{p}_{ij}}{p_{ij}^3} - \frac{\vec{p}_{qj}}{p_{qj}^3}\right) \quad [17]$$

where G is the universal gravitational constant, $\vec{p}_{qi}$ is the position vector from the central body to the particle of interest, and p_{qi} is the norm of this vector. Likewise, $\vec{p}_{ij}$ and $\vec{p}_{qj}$ are position vectors to the perturbing bodies from the particle of interest and the central body, respectively. In this investigation the Earth or Moon are employed as the central body, while the Sun and Jupiter are included as additional perturbing bodies. The locations of these bodies are obtained from the Jet Propulsion Laboratory's Navigation and Ancillary Information Facility (NAIF) SPICE ephemeris data, specifically the DE421 ephemerides.[36] The particle of interest in this application is assumed to be a low-thrust spacecraft with an infinitesimally small mass compared to the masses of the other bodies. Finally, the states of all bodies are expressed in the J2000 inertial frame and the initial epoch is noon UTC on January 1st, 2000. Together, these parameters define the ephemeris model employed to validate trajectories.

IV. Dynamical Structures

Initial low-thrust trajectory designs may exploit a variety of dynamical structures, including both ballistic CR3BP arcs and thrust-enabled motion from the CR3BP-LT. A preliminary understanding of the structures available in any model is available from an analysis of the local linear dynamics near the equilibrium solutions. From this basic analysis, numerical algorithms globalize the local dynamics to yield families of structures, such as periodic and quasi-periodic orbits, that may be employed as destination orbits or as intermediate paths. Finally, dynamical systems techniques are applied to periodic orbits to construct manifolds that offer low-cost transfers into and out of the originating structure. As manifolds exist for both ballistic and low-thrust periodic solutions, they are a valuable component of orbit chains for low-thrust trajectory design.

IV.i Equilibrium Solutions

The planar dynamics in the CR3BP yield equilibrium solutions that supply an initial characterization of the local and global dynamics that may be utilized for path planning. Linearizations of the nonlinear dynamics relative to the equilibria describe local stable, unstable, and center manifolds. Global invariant manifolds are constructed by transitioning the linear results to the nonlinear model, where they are leveraged for trajectory design.[35] The CR3BP admits five equilibrium solutions, the well known *Lagrange points*. Three *collinear* points, i.e., L_1, L_2, and L_3, are located on the x-axis and are characterized by a saddle and a center subspace. Accordingly, stable and unstable manifolds supply transit motion to and from these equilibria (the saddle mode), and oscillatory solutions exist near the fixed point (the center mode). The triangular points, i.e., L_4 and L_5, do not possess a saddle mode and are characterized by a four-dimensional center subspace in the Earth-Moon CR3BP. Subsequently, no manifolds describe flow to or from these fixed points. Periodic and quasi-periodic structures are initialized from linear approximations supplied by the center subspace associated with each equilibrium point, yielding families of structures such as the well-known planar Lyapunov orbits near L_1, L_2, and L_3 and the short period orbits (SPOs) near L_4 and L_5.

Similar to the CR3BP, the planar CR3BP-LT admits equilibrium solutions that supply useful flow characterizations. However, the locations, local linear dynamics, and number of equilibrium points vary with the thrust magnitude and orientation.[34] Subsequently, manipulations of the low-thrust acceleration vector directly influence the existence and characteristics of nearby dynamical structures. When a_{lt} is small, the CR3BP-LT equilibria are located near the natural equilibrium points and are characterized by similar linear modes. However, as a_{lt} increases, the

low-thrust equilibria move further from the natural fixed points and the associated stability characteristics change, both qualitatively (e.g., saddle, center) and quantitatively (e.g., time constant, frequency). These variations between the natural and low-thrust equilibrium solutions supply novel flow patterns that are employed to inform initial guesses for low-thrust transfers.

IV.ii Periodic Solutions

Periodic solutions in the CR3BP are important components of many trajectory design applications as they supply bounded, repeated motion in space while accounting for third-body effects, a level of fidelity not available in the conic model. Additionally, periodic motion from the CR3BP is transitioned to ephemeris models via corrections algorithms.[37] Many families of periodic solutions originate from the equilibrium solutions; very near the fixed point, the nonlinear periodic motion is well approximated by the local linear dynamics of the center subspace. Continuation methods are then employed to compute additional solutions that are affected more strongly by the nonlinearities of the global dynamics. These *families* of dynamical structures are parameterized by a single quantity, such as the Jacobi constant (or, equivalently, H_{nat}), orbit period, or a nonphysical parameter. Accordingly, structures are selected from a family based on the set of characteristics required for a mission application.

Periodic solutions are also available in the CR3BP-LT, with many families of these structures also originating near the low-thrust equilibrium solutions that possess a center subspace. As the equilibria locations and stability properties vary from the natural CR3BP conditions as a function of the low-thrust magnitude, a_{lt}, and orientation, α, families of solutions are available in the CR3BP-LT that do not exist in the natural problem, such as those plotted in Figure 2. Similar to families of orbits in the CR3BP, low-thrust periodic orbit families are parameterized by a single value such as H_{lt}, orbit period, α, or a_{lt}. For example, the family of orbits in Figure 2 evolves with α; each family member is characterized by the same $H_{lt} = -1.453$ value. Each orbit within this family is also a member of a family that evolves through a range of H_{lt} values with a fixed α value. Thus, given the increased dimension of the CR3BP-LT, families may be continued along a greater number of dimensions, yielding a larger set of solutions for use in an initial trajectory design. Furthermore, as α and a_{lt} are both available as continuation parameters, links between the spacecraft thrust history and trajectory geometry are available from these solutions.

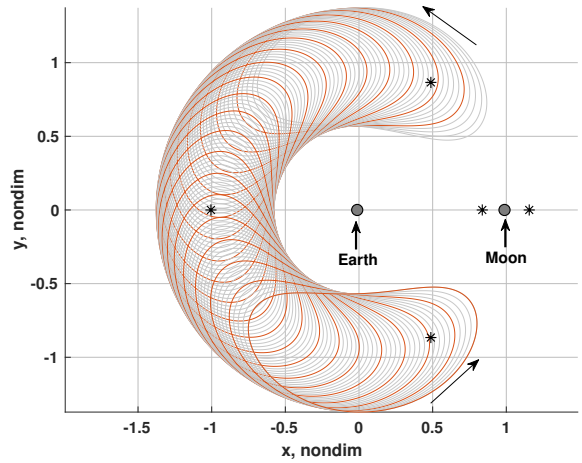

Fig. 2: Family of periodic orbits in the Earth-Moon CR3BP-LT for $a_{lt} = 7\text{e-}2$ and $H_{lt} = -1.453$; each family member corresponds to a different α value; some members are colored to emphasize the orbit geometry

IV.iii Manifolds

Invariant manifolds associated with periodic orbits describe flow through the CR3BP.[38] Similar to the equilibrium solutions, linear dynamics derived from the stroboscopic representation of a periodic orbit may be characterized as saddle modes with stable and unstable manifolds, or as center modes that indicate additional oscillatory motion, i.e., quasi-periodic solutions. As the stable and unstable manifolds asymptotically approach the periodic solution in reverse and forward time, respectively, they are frequently exploited as pathways between periodic structures, including for missions like GENESIS.[39] The manifolds associated with a periodic orbit, by necessity, are characterized by the same properties as the originating structure. That is, manifolds of a CR3BP orbit possess the same H_{nat} value as the orbit, and manifolds of a CR3BP-LT orbit are characterized by the same H_{lt}, α, and a_{lt} values as the low-thrust periodic structure. Accordingly, the manifolds associated with low-thrust periodic orbits (LTPOs) supply additional links between geometric paths through space and specific sets of control parameters (α and a_{lt}), facilitating the construction of an initial transfer design with a priori knowledge of the thrust profile.

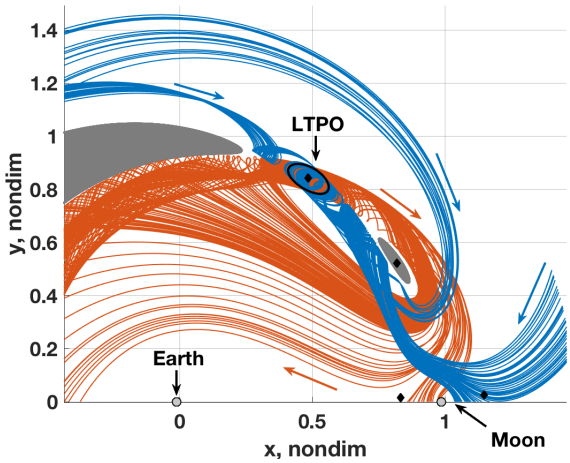

Fig. 3: Stable (blue) and unstable (orange) manifolds associated with a low-thrust periodic orbit (LTPO) in the Earth-Moon CR3BP-LT for a_{lt} = 7e-2, $\alpha = 60°$, and $H_{lt} = -1.562$. Forbidden regions corresponding to this H_{lt} value (gray regions) bound the low-thrust motion; low-thrust equilibria are plotted as black diamonds

V. Results

Dynamical structures from the CR3BP and CR3BP-LT are combined in chains to design transfers for two different applications. In each application, a chain of only natural structures and a chain with structures from both models are utilized as initial designs for the direct transcription algorithm. The objective function for this algorithm is maximum final mass, and the total change in mass along a trajectory, Δm, is one of the parameters used to compare results. Other characteristics such as geometry and thrust profile are also employed to draw comparisons and explore the effects of the low-thrust structures on the optimal trajectory delivered by direct transcription. These comparisons reveal that low-thrust structures effect the final, optimal path in similar ways as natural dynamical structures. Thus, when the geometries of two orbit chains are similar (regardless of which model the component structures are obtained from), comparable optimal solutions are computed, as demonstrated in the first application. Within this investigation, solutions with broadly similar characteristics are described as falling in the same optimal "basins". This application of the term basin is looser than the mathematical definition of the word; however, in this context, it is a useful term for grouping the types of optimal solutions that result from a variety of initial trajectory designs. In the second application, two initial designs with significantly different geometries yield significantly different optimal solutions, that is, two solutions that appear to fall within different optimal basins. A valuable implication of this framework is that when the available basins of solutions for a type of transfer are understood, then it is possible to construct an initial design that generates a solution with the features of a specific basin. The versatility of this methodology is extended when low-thrust structures are included in an initial guess, because these structures offer novel geometries for some applications. Thus, the optimal solution can be intentionally biased by selecting low-thrust arcs with desirable properties, as demonstrated in the second application.

V.i Application 1: L_4 SPO to L_3 Lyapunov Transfer

Families of low-thrust periodic orbits offer new geometries and energy profiles that may be employed to aid the process of low-thrust trajectory design. Moreover, in contrast to natural dynamical structures, low-thrust dynamical structures include prescribed control histories, and these may offer an improved initial guess for the control profile necessary to achieve a feasible trajectory. In this sample application, members of a family of low-thrust periodic orbits are utilized in an orbit chain technique to compose an initial guess for a low-thrust transfer from an L_4 short period orbit (SPO) to an L_3 Lyapunov orbit, both characterized by the natural Hamiltonian value $H_{nat} = -1.453$. To offer a comparison, the same transfer is developed using an orbit chain consisting of only natural dynamical structures from the CR3BP as an initial guess. Contrasting the results of the two different initial guesses indicates how using low-thrust dynamical structures in the transfer design process affects the final trajectory.

An orbit chain consisting of only natural dynamical structures from the CR3BP is assembled as an initial guess for the transfer between the aforementioned L_4 SPO and L_3 Lyapunov orbits. The transfer computed from this initial guess offers a baseline to assess the influence of low-thrust dynamical structures in an initial guess on the converged feasible and optimal solutions. In addition to the initial and final orbits, several other members of the L_4 SPO and L_3 Lyapunov orbit families are included as intermediate links in the orbit chain, as seen in Figure 4(a). These additional links are added to reduce the discontinuities in position and velocity between subsequent members of the orbit chain. The inclusion of these supplementary links necessitates a change in energy,

demonstrated in Figure 4(b) with a plot of H_{lt} as a function of orbital period for the L_4 SPO and L_3 Lyapunov families. Note that the low-thrust Hamiltonian is equivalent to the natural Hamiltonian, H, for natural arcs as the low-thrust acceleration magnitude, a_{lt}, is zero, negating the extra terms in Equation [10]; H_{lt} is used for consistency when both low-thrust and natural arcs are included in the chain. Figure 4(b) illustrates that the additional members of the L_4 SPO family increase the value of H_{lt} with increasing distance from the originating SPO, while the extra L_3 Lyapunov orbits decrease this value again with decreasing distance to the destination Lyapunov. Furthermore, the third and fourth orbit chain links are selected to possess the same H_{lt} value, to reduce the energy change required to transition between periodic orbit families. More intermediate links, including additional orbits from either the L_4 SPO or L_3 Lyapunov orbit families, could be added to further reduce discontinuities; however, the inclusion of additional orbits yields an increased time of flight and a larger number of design variables in the optimization problem. Rather, it is advantageous to include alternative dynamical structures that offer paths that span the region of interest and reduce the discontinuities observed within the initial guess.

As an alternative to a chain of purely ballistic arcs, an orbit chain that leverages a unique family of L_4 LTPOs is assembled to assess whether this novel approach can supply an initial guess with reduced state discontinuities and lead to a more optimal solution. The family of L_4 LTPOs utilized in this transfer is defined by $H_{lt} = -1.453$ and is displayed in Figure **??**. This family of LTPOs is selected because its members neatly span the space between the natural departure and destination orbits. Therefore, four orbits from this family are employed in an orbit chain that also includes the natural initial and final orbits. Figure 5(a) illustrates how the consecutive links of this orbit chain overlap at multiple points in position space, and that the intermediate links gradually transition the direction of velocity from the departure to the destination orbits. Not only do these LTPOs offer reduced position and velocity discontinuities between orbit chain links, but they also maintain a value of H_{lt} consistent with the initial and final orbits, as seen in Figure 5(b). As the H_{lt} value of each low-thrust periodic orbit is consistent with the initial and final natural orbits, the size of and velocity along each of the links are similar. These similarities facilitate convergence and offer an alternative geometry compared to the stack of natural orbits in Figure 4(a). A

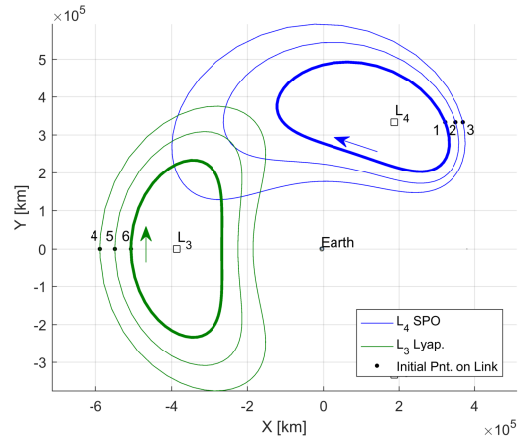

(a) Selected members of the L_4 SPO and L_3 Lyapunov orbit families including the initial and final orbits (bolded).

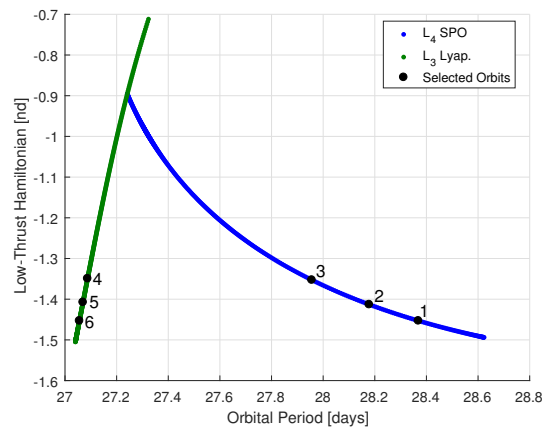

(b) Plot of H_{lt} as a function of orbital period for the orbit families used to construct initial guess.

Fig. 4: Natural periodic orbits are employed to compose an initial guess for a transfer from an L_4 SPO to an L_3 Lyapunov orbit. Geometry and energy characteristics are examined to select the components of the initial guess.

chain constructed from arcs with similar energy values may yield a transfer with lower propellant costs, but other variables (orbit orientation, velocity direction) strongly influence convergence and the resulting optimal solution.

Finally, the two different orbit chains are used as initial guesses for the direct transcription algorithm and the results are compared to assess the effect of the various orbit chain links on the characteristics of the resulting solution. Despite the significant differences between the initial guesses displayed in Fig-

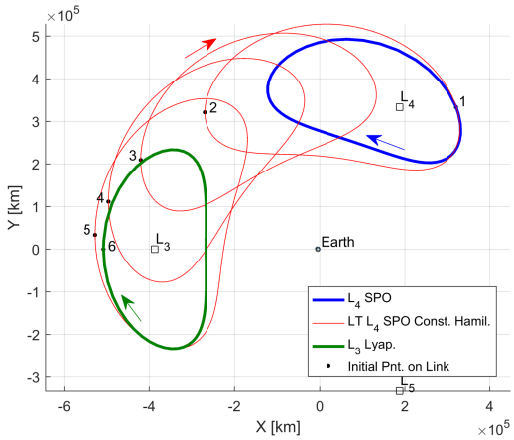

(a) Selected members of a low-thrust L_4 SPO family at $H_{lt} = -1.453$ along with the departure L_4 SPO and arrival L_3 Lyapunov (bolded).

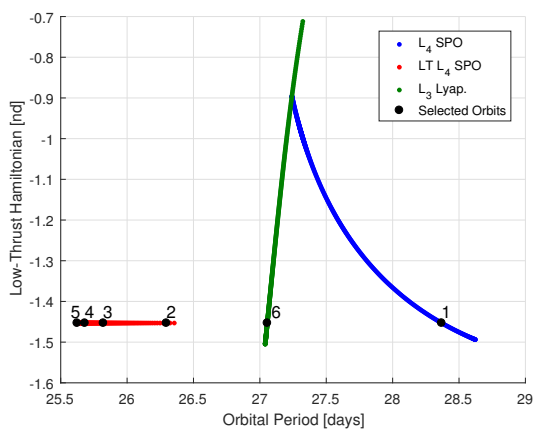

(b) Plot of H_{lt} as a function of orbital period for the orbit families employed to construct initial guess.

Fig. 5: Low-thrust periodic orbits are employed to compose an initial guess for a transfer from an L_4 SPO to an L_3 Lyapunov orbit. Geometry and energy characteristics are examined to select the components of the initial guess.

ures 4 and 5, the mass optimal transfers computed from each guess are quite similar, as seen in Figure 6. Both transfers exhibit nearly identical geometries with thrust segments in very similar locations. Both utilize brief thrust segments for departure and insertion as well as two longer thrust segments during intermediate arcs. The small differences between the two solutions become more clear when their energy profiles, plotted in Figure 7, are examined. These profiles display H_{lt} as a function of time of flight for both transfers. While these profiles are very similar, it is evident that the transfer generated with the orbit chain composed of only natural dynamical structures deviates more frequently and farther from the H_{lt} value of the initial and final orbits. Prior to the first long duration burn, the energy profile in Figure 7(a) deviates from the initial value of H_{lt} more significantly than the profile in Figure 7(b) which corresponds to the solution initialized with low-thrust structures. Furthermore, the coast arc bounded by the two long duration burns maintains a lower energy level for the transfer computed using only natural orbits; this difference corresponds to the slight variation in geometry for this arc between the two solutions (shown in Figure 6). A transfer with minimal energy changes corresponds to the theoretical minimum-cost path, and this is likely the reason that the transfer generated using LTPOs requires a smaller Δm. The change in mass associated with both transfers computed in the CR3BP is summarized along with time of flight (TOF) and ΔV in Table 1. The reported ΔV values are computed with the classical rocket equation. This expression offers an approximation of the equivalent ΔV required for the low-thrust transfer.

The transfer generated with the aid of low-thrust dynamical structures consumes over 2 kilograms less propellant, which translates to a ΔV savings of approximately 65 m/s. It is possible that the nearly constant energy profile of the initial guess that includes low-thrust dynamical structures may have guided the optimizer to a slightly more optimal solution. However, this sample application alone is not sufficient to state that these structures generally lead to superior mass optimal solutions. The similarities between the two solutions – despite the significantly different initial guesses – highlights the robustness of the direct transcription algorithm. Moreover, this result is consistent with previous work that demonstrates both the existence of multiple "basins" of optimal solutions and how the components of an orbit chain guide the optimal solution into one of these basins[7]. In this application, the orbit chains are similar enough that they lead to similar local optimal basins. However, if a resonant orbit that first passes near the Moon before returning to the vicinity of L_3 is included in the orbit chain instead, the resulting solution will follow a similar trajectory. Thus, the results of this application, understood in the context of optimal basins, reveal that although dynamical structures from the CR3BP-LT offer novel geometries, these structures may still lead to a similar set of basins. Hence, the initial guesses with and without LTPOs in this case result in comparable optimal

Init. Guess	TOF $[days]$	Δm $[kg]$	ΔV $[m/s]$
Nat. Only	165.716	5.825	171.887
With LT	158.847	3.572	105.289

Table 1: Summary of key parameters for the low-thrust transfers computed in the Earth-Moon CR3BP for Application 1.

paths. However, the framework of optimal basins also underscores a potential advantage of utilizing low-thrust dynamical structures: Due to their unique characteristics (e.g., geometry, location, energy), including these structures in an orbit chain may guide the solution towards a different basin that cannot be easily accessed with an initial guess composed of natural structures alone. Indeed, such a result is presented in the following section.

Finally, to validate that these transfers and the methods employed to compute them are available for practical applications, both low-thrust transfers are transitioned to an N-body ephemeris model that includes the Earth, Moon, Sun, and Jupiter. The resulting transfers are displayed in Figure 8. Clearly, both transfers retain a similar geometry to what was observed in the CR3BP results. This result indicates that similar trajectories are available in an ephemeris model and may be leveraged in realistic mission scenarios.

V.ii Application 2: L_4 SPO to L_1 Lyapunov Transfer

Low-thrust structures offer unique paths that may differ significantly from the natural dynamics. For example, unstable LTPOs exist in the vicinity of stable natural periodic orbits. Accordingly, transfers to the natural periodic orbit can be facilitated by the LTPO stable and unstable manifolds that flow into and out of the region. To illustrate a transfer leveraging these structures, a trajectory is designed to deliver a spacecraft from an L_4 SPO with $H_{nat} = -1.487$ to an L_1 Lyapunov orbit with $H_{nat} = -1.503$. An orbit chain technique is utilized to construct two different initial designs: (i) a chain of purely natural orbits and their associated manifolds, and (ii) a chain that includes natural orbits and the manifold of a nearby L_4 LTPO. Once an initial guess is constructed, a direct transcription algorithm is employed to remove discontinuities in the solution, yielding a feasible design. Finally, the feasible solution is optimized to maximize the final spacecraft mass, and the solutions resulting from the two initial designs are compared.

An orbit chain that delivers the spacecraft from

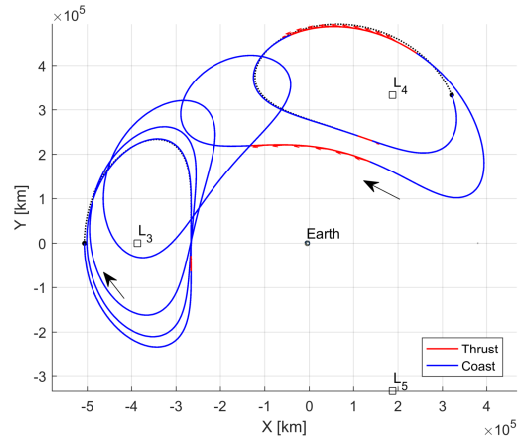

(a) Transfer from orbit chain initialized from only natural dynamical structures.

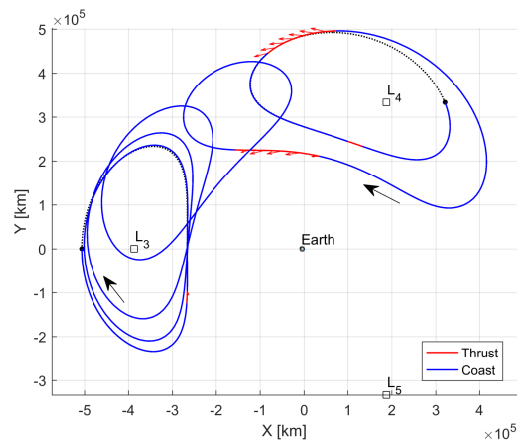

(b) Transfer from orbit chain initialized with low-thrust periodic orbits.

Fig. 6: Direct transcription is employed to compute mass optimal low-thrust transfers using the orbit chain initial guesses.

the L_4 SPO to the L_1 Lyapunov is first constructed leveraging only dynamical structures from the natural CR3BP. Stable manifolds associated with the L_1 orbit, plotted in Figure 9(a), pass near the L_4 SPO and offer a suitable geometry to facilitate the transfer. However, while these natural manifolds are located near the L_4 orbit in position space, a large velocity discontinuity, i.e., an H_{nat} discontinuity, exists between the L_1 Lyapunov manifolds and the SPO. As the L_4 orbit is stable and does not possess manifolds, no additional natural structures to guide flow between the two orbits are immediately apparent. To complete the transfer design, five revolutions along the initial L_4 orbit and a single revolution of the L_1

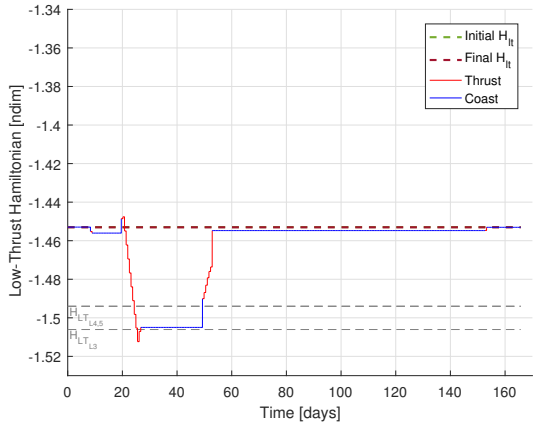

(a) Optimal transfer generated with natural dynamical structures.

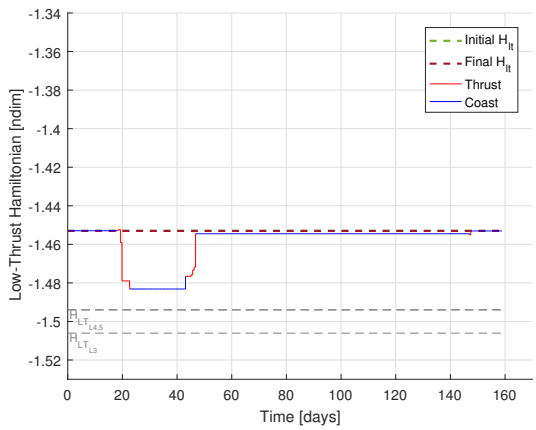

(b) Optimal transfer generated with low-thrust dynamical structures.

Fig. 7: The time history of the low-thrust Hamiltonian, H_{lt}, for each transfer offers insight on how low-thrust maneuvers change the energy of the spacecraft to achieve the transfer

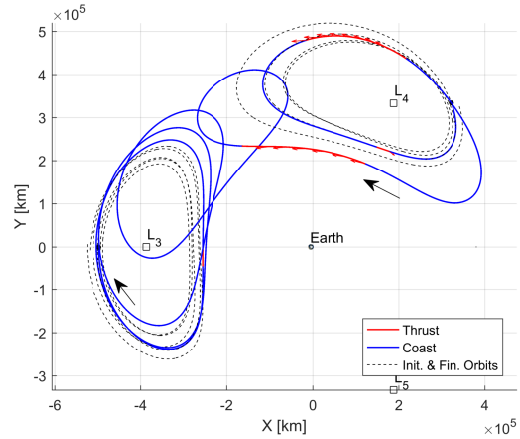

(a) Transfer generated with natural dynamical structures.

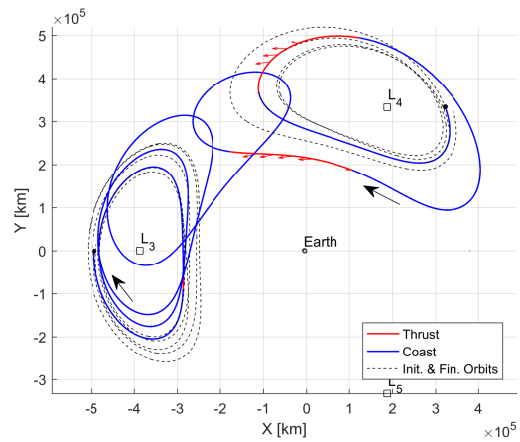

(b) Transfer generated with low-thrust dynamical structures.

Fig. 8: Direct transcription is employed to compute mass optimal low-thrust transfers in an N-Body ephemeris model using the CR3BP result as an initial guesses.

orbit are included. The five revolutions along the SPO are included so that the transfer time of flight (TOF) is similar to the design that utilizes a low-thrust manifold. In addition to adding transfer time, this stacking supplies ample time and space for the spacecraft to make the required energy change between the L_1 manifold and the L_4 SPO, facilitating convergence in the direct transcription algorithm.

The second transfer design offers an alternate geometry by leveraging low-thrust dynamical structures. While H_{nat} is constant on every natural structure, the addition of low-thrust causes an evolving H_{nat} value along low-thrust dynamical structures (H_{lt}, on the other hand, remains constant). Accordingly, both geometric and energetic paths may be incorporated with low-thrust structures. To accomplish the L_4 to L_1 transfer, an unstable LTPO with a similar geometry and energy as the natural L_4 SPO is identified to reduce position and velocity discontinuities between the two structures. The manifolds of this low-thrust orbit, plotted in Figure 9(b), offer an alternative set of paths in position space to complete the transfer. To design the transfer, a single revolution of the natural L_4 SPO is included, followed by a manifold originating from the nearby L_4 LTPO and then two revolutions of the natural L_1 Lyapunov

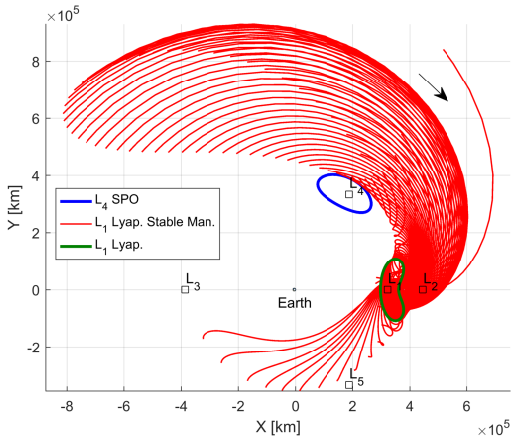

(a) Stable manifolds of an L_1 Lyapunov orbit with $H_{nat} = -1.503$ approach the L_4 SPO in reverse time.

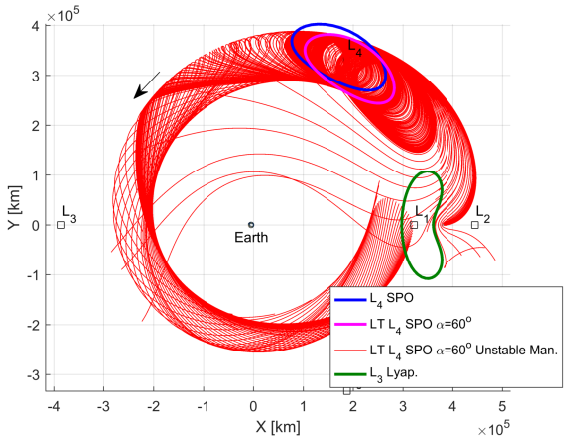

(b) Unstable manifolds of a low-thrust L_4 LTPO with $\alpha = 60^o$ and $H_{lt} = -1.553$ approach the lunar region from two directions.

Fig. 9: The invariant manifolds of a low-thrust L_4 LTPO offer different geometries than those of the destination L_1 Lyapunov manifold.

orbit.

In both scenarios, the manifold path best suited for a given orbit chain is chosen by inspecting the total set of stable or unstable manifolds and identifying the manifold that demonstrates the closest intersection in position space with the adjacent orbit in the chain. Additionally, the direction and magnitude of the velocity vector at the end of the manifold is selected to be similar to the point on the final orbit that the manifold intersects. The velocity states are directly considered in this case, rather than the analogous energy values examined in the previous application, because of the critical importance of matching velocity direction when linking the manifolds to another dynamical structure. This change in strategy is necessary because invariant manifolds at the same value of H_{nat} or H_{lt} can exhibit wildly different position and velocity profiles, therefore it is necessary to carefully consider these state differences when assembling an orbit chain to ensure the initial guess contains reasonably small discontinuities.

Following the prescribed manifold selection strategy, the initial designs for each transfer are constructed. The all-natural design, plotted in Figure 10(a), includes a direct path between the two periodic orbits via an L_1 stable manifold arc. The low-thrust design, seen in Figure 10(b), leverages a low-thrust manifold that encircles the Earth before reaching the destination L_1 orbit. Both initial guesses are converged via direct transcription, first for feasibility, and then for mass-optimality. The final, optimized results, plotted in Figure 11, possess distinctly different geometries that are biased by the initial designs. The solution initialized with only natural structures, seen in Figure 11(a), approximately mirrors the initial geometry (Figure 10(a)) with a transfer approaching the L_1 Lyapunov from the right, consistent with the L_1 stable manifold. The solution leveraging low-thrust structures, plotted in Figure 11(b), also remains generally consistent with the initial geometry (Figure 10(b)), approaching the Lyapunov orbit from the left after encircling the Earth. As expected, the structure of the initial guess biases the solution towards particular characteristics.

Comparison of the optimal low-thrust transfers displayed in Figure 11 reveals the influence of the different initial guesses and the benefits offered by including low-thrust dynamical structures. When only natural structures are included in the initial guess, the resulting transfer, shown in Figure 11(a), utilizes an extended thrust segment near the initial L_4 SPO to depart this orbit and another brief thrust arc to connect with the stable manifold of the L_1 Lyapunov orbit. The initial revolution of the L_4 SPO employed in the initial guess remains in place, while the subsequent stacked revolutions are spread over the L_4 region to facilitate the connection with the stable manifold. The time of flight of this transfer is about 205 days; a transfer with a shorter TOF is likely available if the initial guess is modified to include fewer revolutions of the L_4 SPO.

The transfer constructed with low-thrust dynamical structures, displayed in Figure 11(b), also exhibits loops near L_4 because the low-thrust periodic orbit and manifold included in the initial guess possess this

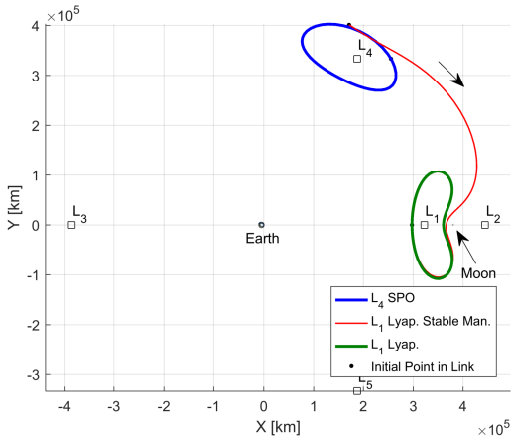

(a) Orbit chain with only natural dynamical structures

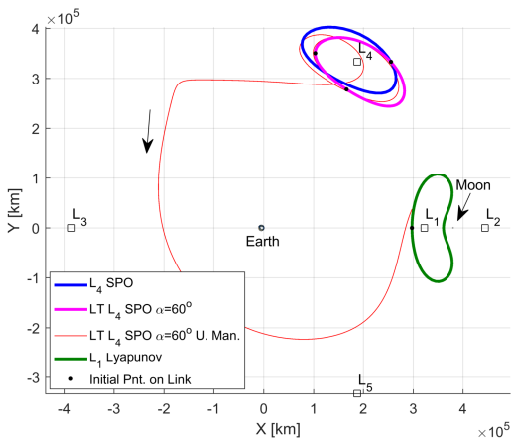

(b) Orbit chain with low-thrust dynamical structures

Fig. 10: The orbit chain approach is employed to construct two different initial guesses for the desired transfer. The first leverages only natural dynamical structures while the second includes low-thrust structures. Both orbit chains exploit invariant manifolds.

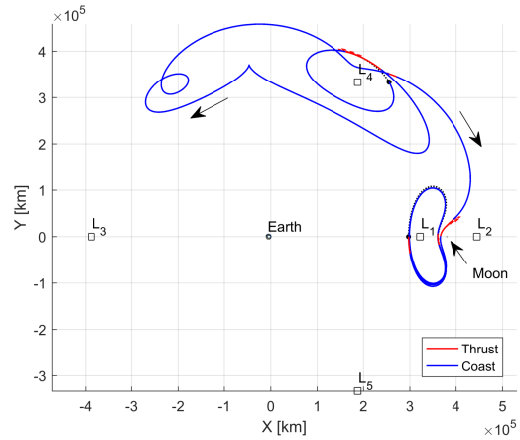

(a) Transfer from orbit chain with only natural dynamical structures

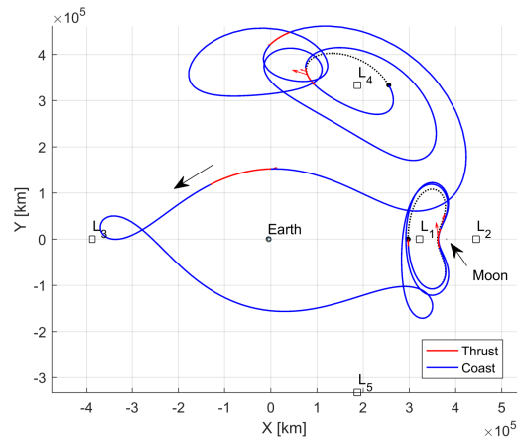

(b) Transfer from orbit chain with low-thrust dynamical structures

Fig. 11: Direct transcription is employed to compute mass optimal low-thrust transfers using the orbit chain initial guesses.

motion. The time of flight of this transfer is approximately 201 days, consistent with the initial design. The geometric and time of flight differences of the two transfers lead to different propellant usages: 2.422 kg and 1.518 kg (for a 1000 kg spacecraft) for the natural and low-thrust seeded designs, respectively. These differences, summarized in Table 2, may lie within the variability of the solution due to numerical considerations such as node placement. Nonetheless, the transfer generated using low-thrust dynamical structures does require less propellant and ΔV than the alternate case. In addition to this quantitative difference, the inclusion of low-thrust structures also enables an alternative transfer geometry that is well-predicted by the initial design. In this case, the low-thrust manifold geometry is not straightforwardly available from the natural dynamical structures of interest, i.e., the L_1 Lyapunov, its manifolds, and L_4 SPO. The novel geometries, and, in some cases, improved optimal solutions, indicate the benefit of incorporating low-thrust dynamical structures in the transfer design process.

Finally, to validate that these transfers and the methods employed to compute them are available for practical applications, both low-thrust transfers are transitioned to an N-body ephemeris model that in-

Init. Guess	TOF $[days]$	Δm $[kg]$	ΔV $[m/s]$
Nat. Only	205.188	2.422	71.331
With LT	200.756	1.518	44.694

Table 2: Summary of key parameters for the low-thrust transfers computed in the Earth-Moon CR3BP for Application 2.

cludes the Earth, Moon, Sun, and Jupiter. The resulting transfers are displayed in Figure 12. Clearly, both transfers retain a similar geometry to what was observed in the CR3BP results. This result indicates that similar trajectories are available in an ephemeris model and may be leveraged in realistic mission scenarios.

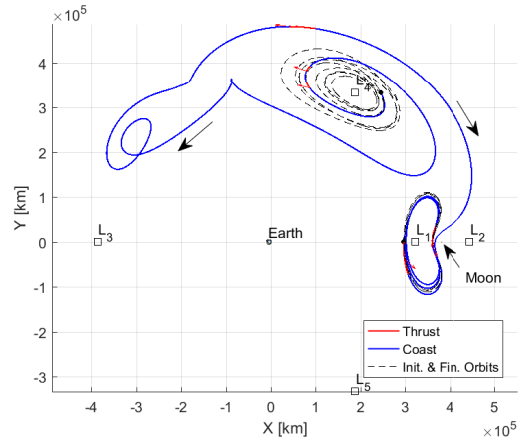

(a) Transfer generated with natural dynamical structures.

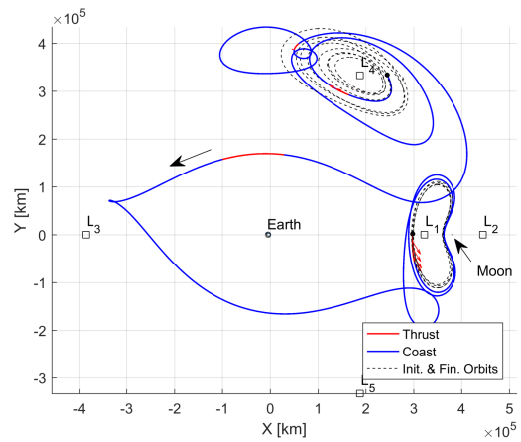

(b) Transfer generated with low-thrust dynamical structures.

Fig. 12: Direct transcription is employed to compute mass optimal low-thrust transfers in an N-Body ephemeris model using the CR3BP result as an initial guesses.

VI. Concluding Remarks

An orbit chain approach to low-thrust trajectory design enables rapid exploration of the design space afforded by a given dynamical model. Experimentation with the various combinations of dynamical structures that may be included in an orbit chain often reveals different local "basins" of optimal solutions. This investigation demonstrates that dynamical structures generated in the CR3BP-LT can be incorporated into an orbit chain technique in the same manner as natural periodic orbits and manifolds. Through the application of dynamical systems theory to the CR3BP-LT, low-thrust enabled dynamical structures with novel geometries and energy profiles may be generated. The new catalog of low-thrust periodic orbits and manifolds offered by the CR3BP-LT permits the assembly of initial guesses with reduced state discontinuities or gaps in energy level, as seen in the first sample application. However, this application also illustrates that, despite their unique properties, the inclusion of low-thrust dynamical structures in an orbit chain can lead to an optimal solution that is nearly identical to the one computed with an initial guess composed of only natural dynamical structures. Conversely, the second sample application shows that a drastically different local optimal is obtained when a low-thrust dynamical structure with a very different geometry is utilized. Furthermore, this application utilizes a manifold from a low-thrust enabled variant of a naturally stable periodic orbit, and, this alone demonstrates the utility of employing low-thrust dynamical structures for trajectory design. Overall, low-thrust dynamical structures offer a new catalog of options that may be leveraged in an orbit chain technique for the computation of optimal low-thrust trajectories. This new array of options expands the design space by enabling low-thrust trajectories with different times of flight, propellant consumption, or geometric characteristics to be computed.

Acknowledgements

This research is supported by NASA Space Technology Research Fellowships, NASA Grants NNX16AM42H and NNX16AM40H. Portions of this work were carried out at the NASA Goddard Space Flight Center. Additionally, portions of this work

were completed at the Jet Propulsion Laboratory, California Institute of Technology, under a contract with the National Aeronautics and Space Administration. Government sponsorship acknowledged. © 2018. All rights reserved. The authors wish to thank the Purdue University School of Aeronautics and Astronautics for their facilities and support, including access to the Rune and Barbara Eliasen Visualization Laboratory. Additionally, many thanks to the Purdue Multi-Body Dynamics Research Group for interesting discussions and ideas.

References

[1] M. D. Rayman, P. Varghese, D. H. Lehman, and L. L. Livesay. Results from the Deep Space 1 Technology Validation Mission. *Acta Astronautica*, 47(2-9):475–487, 2000.

[2] C. Russell and C. Raymond, editors. *The Dawn Mission to Minor Planets 4 Vesta and 1 Ceres*. Springer-Verlag, New York, 1 edition, 2012. ISBN 978-1-4614-4902-7.

[3] N. Bosanac, A. D. Cox, K. C. Howell, and D. C. Folta. Trajectory design for a cislunar CubeSat leveraging dynamical systems techniques: The Lunar IceCube mission. *Acta Astronautica*, 144: 283–296, 2018.

[4] D. Y. Oh, S. Collins, D. Goebel, B. Hart, G. Lantoine, S. Snyder, G. Whiffen, L. Elkins-tanton, P. Lord, Z. Pirkl, and L. Rotlisburger. Development of the Psyche Mission for NASA's Discovery Program. In *35th International Electric Propulsion Conference*, pages 1–19, Atlanta, Georgia, 2017.

[5] M. L. Mcguire, L. M. Burke, S. L. McCarty, K. J. Hack, R. J. Whitley, D. C. Davis, and C. Ocampo. Low Thrust Cis-Lunar Transfers Using a 40 kW-Class Solar Electric Propulsion Spacecraft. In *AAS/AIAA Astrodynamics Specialist Conference 2017*, pages 1–21, Stevenson, Washington, 2017.

[6] R. E. Pritchett, K. C. Howell, and D. J. Grebow. Low-Thrust Transfer Design Based on Collocation Techniques: Applications in the Restricted Three-Body Problem. In *AAS/AIAA Astrodynamics Specialist Conference*, pages 1–20, Stevenson, Washington, 2017.

[7] R. E. Pritchett, E. Zimovan, and K. Howell. Impulsive and Low-Thrust Transfer Design Between Stable and Nearly-Stable Periodic Orbits in the Restricted Problem. *2018 Space Flight Mechanics Meeting*, 2018.

[8] K. C. Howell, B. T. Barden, and M. W. Lo. Application of Dynamical Systems Theory to Trajectory Design for a Libration Point Mission. *The Journal of the Astronautical Sciences*, 45(2): 161–178, 1997.

[9] W. S. Koon, M. W. Lo, J. E. Marsden, and S. D. Ross. Heteroclinic connections between periodic orbits and resonance transitions in celestial mechanics. *Chaos: An Interdisciplinary Journal of Nonlinear Science*, 10(2):427–469, 2000.

[10] G. Gómez, W. S. Koon, M. W. Lo, J. E. Marsden, J. J. Masdemont, and S. D. Ross. Connecting orbits and invariant manifolds in the spatial restricted three-body problem. *Nonlinearity*, 17 (5):1571–1606, 2004.

[11] S. Ross and M. Lo. The lunar l1 gateway-portal to the stars and beyond. In *AIAA Space 2001 Conference and Exposition*, page 4768, 2001.

[12] M. Vaquero and K. C. Howell. Leveraging Resonant-Orbit Manifolds to Design Transfers Between Libration-Point Orbits. *Journal of Guidance, Control, and Dynamics*, 37(4):1143–1157, 2014.

[13] A. F. Haapala and K. C. Howell. A Framework for Constructing Transfers Linking Periodic Libration Point Orbits in the Spatial Circular Restricted Three-Body Problem. *International Journal of Bifurcation and Chaos*, 26(05): 1630013, 2016.

[14] J. S. Parker, K. E. Davis, and G. H. Born. Chaining periodic three-body orbits in the Earth-Moon system. *Acta Astronautica*, 67(5-6):623–638, 2010.

[15] M. W. Lo and J. S. Parker. Chaining Simple Periodic Three Body Orbits. In *AAS/AIAA Astrodynamics Specialist Conference*, pages 1–16, Lake Tahoe, CA, 2005.

[16] R. L. Restrepo and R. P. Russell. A Database of Planar Axi-Symmetric Periodic Orbits for the Solar System. *AAS Astrodynamics Specialists Conference*, pages 1–20, 2017.

[17] R. L. Restrepo and R. P. Russell. Patched Periodic Orbits: A Systematic Strategy for Low Energy Transfer Design. *AAS Astrodynamics Specialists Conference*, pages 1–20, 2017.

[18] M. Canon, C. Cullum, and E. Polak. *Theory of Optimal Control and Mathematical Programming*. McGraw-Hill, New York, 1970.

[19] D. J. Grebow and T. A. Pavlak. MColl: Monte Collocation Trajectory Design Tool. In *AAS/AIAA Astrodynamics Specialist Conference*, pages AAS 17–776, Stevenson, Washington, 2017.

[20] J. T. Betts. Survey of Numerical Methods for Trajectory Optimization. *Journal of Guidance, Control, and Dynamics*, 21(2):193–207, 1997.

[21] F. Topputo and C. Zhang. Survey of Direct Transcription for Low-Thrust Space Trajectory Optimization with Applications. *Abstract and Applied Analysis*, 2014:15, 2014.

[22] B. A. Conway. A Survey of Methods Available for the Numerical Optimization of Continuous Dynamic Systems. *Journal of Optimization Theory and Applications*, 152(2):271–306, 2012.

[23] M. T. Ozimek, D. J. Grebow, and K. C. Howell. A Collocation Approach for Computing Solar Sail Lunar Pole-Sitter Orbits. *Open Aerospace Engineering Journal*, 3:65–75, 2010.

[24] M. T. Ozimek. *Low-Thrust Trajectory Design and Optimization of Lunar South Pole Coverage Missions*. Ph.d. dissertation, Purdue University, 2010.

[25] J. F. C. Herman. *Improved Collocation Methods to Optimize Low-Thrust , Low-Energy Transfers in the Earth-Moon System by*. Ph.d., University of Colorado, Boulder, CO, 2015.

[26] N. L. Parrish, J. S. Parker, S. P. Hughes, and J. Heiligers. Low-Thrust Transfers From Distant Retrograde Orbits To L2 Halo Orbits in the Earth-Moon System. In *International Conference on Astrodynamics Tools and Techniques*, pages 1–9, Darmstadt, Germany, 2016.

[27] A. Petropoulous and J. Sims. A review of some exact solutions to the planar equations of motion of a thrusting spacecraft. In *2nd International Symposium on Low Thrust Trajectories*, Toulouse, France, June 2002.

[28] S. Hernandez. *Low-Thrust Trajectory Design Techniques with a Focus on Maintaining Constant Energy*. PhD thesis, University of Texas at Austin, Austin, Texas, August 2014.

[29] C. R. McInnes, A. J. C. McDonald, J. F. L. Simmons, and E. W. MacDonald. Solar sail parking in restricted three-body systems. *Journal of Guidance, Control, and Dynamics*, 17(2), March-April 1994.

[30] A. Farrés and À. Jorba. Solar sail surfing along families of equilibrium points. *Acta Astronautica*, 63:249–257, July 2008.

[31] A. Farrés and À. Jorba. Periodic and quasi-periodic motions of a solar sail close to sl_1 in the earth-sun system. *Celestial Mechanics and Dynamical Astronomy*, 107(1-2):233–253, June 2010.

[32] A. Farrés. Transfer orbits to l4 with a solar sail in the earth-sun system. *Acta Astronautica*, 137: 78–90, 2017.

[33] A. D. Cox, K. C. Howell, and D. Folta. Dynamical structures in a combined low-thrust multi-body environment. In *AAS/AIAA Astrodynamics Specialist Conference*, Columbia River Gorge, Stevenson, Washington, August 2017.

[34] A. D. Cox, K. C. Howell, and D. Folta. Trajectory design leveraging low-thrust, multi-body equilibria and their manifolds. In *AAS/AIAA Astrodynamics Specialist Conference*, Snowbird, Utah, August 2018.

[35] V. Szebehely. *Theory of Orbits: The Restricted Problem of Three Bodies*. Academic Press, 1967.

[36] C. H. Acton. Ancillary data services of nasas navigation and ancillary information facility. *Planetary and Space Science*, 44(1):65–70, 1996.

[37] D. A. D. Tos and F. Topputo. Trajectory refinement of three-body orbits in the real solar system model. *Advances in Space Research*, 59 (8):2117 – 2132, 2017.

[38] W. S. Koon, M. W. Lo., J. E. Marsden, and S. D. Ross. *Dynamical Systems, the Three-Body Problem and Space Mission Design*. Springer, New York, 2011.

[39] M. W. Lo, B. G. Williams, W. E. Bollman, D. Han, Y. Hahn, J. L. Bell, E. A. Hirst, R. A. Corwin, P. E. Hong, K. C. Howell, B. T. Barden, and R. S. Wilson. Genesis mission design. *The Journal of Astronautical Sciences*, 49 (1):169–184, 2001.